2012

Wormholes in de Sitter branes

PHYSICAL REVIEW D, COLLEGE PK, v. 86, n. 2, supl. 2, Part 3, pp. 977-981, 39995, 2012
http://www.producao.usp.br/handle/BDPI/33433

PHYSICAL REVIEW D **86,** 024015 (2012)

Wormholes in de Sitter branes

C. Molina*

Escola de Artes, Ciências e Humanidades, Universidade de São Paulo and Av. Arlindo Bettio 1000, CEP 03828-000, São Paulo-SP, Brazil

J. C. S. Neves†

Instituto de Física, Universidade de São Paulo, C. P. 66318, 05315-970, São Paulo-SP, Brazil

(Received 5 April 2012; published 9 July 2012)

In this work, we present a class of geometries which describes wormholes in a Randall-Sundrum brane model, focusing on de Sitter backgrounds. Maximal extensions of the solutions are constructed and their causal structures are discussed. A perturbative analysis is developed, where matter and gravitational perturbations are studied. Analytical results for the quasinormal spectra are obtained and an extensive numerical survey is conducted. Our results indicate that the wormhole geometries presented are stable.

DOI: 10.1103/PhysRevD.86.024015 PACS numbers: 04.20.Jb, 04.50.Gh, 04.50.Kd

I. INTRODUCTION

Wormholes are compact space-times with nontrivially topological interiors and topologically simple boundaries. They can be seen as connections between different universes or topological handles between distant parts of the same universe. Although they are certainly exotic structures, they appear as exact solutions of Einstein equations with physically relevant scenarios and are compatible with the usual local physics [1]. Samples of the work developed include solutions in usual general relativity [1–5], in Gauss-Bonnet theory [6,7], in Brans-Dicke theory [8–12], and brane world context [13–16].

One motivation in the treatment of wormhole physics was due to the results of Morris, Thorne, and Yurtsever [2,3], which connected time machines and traversable wormholes. More recently, new cosmological observations and theoretical proposals have motivated a renewed interest in geometries which describe Lorentzian wormholes. One of their general characteristics is that wormholes must be supported by "exotic matter," which violates usual energy conditions. Nevertheless, recent observations suggest that the Universe may be dominated by some form of exotic matter [17,18], which makes wormhole scenarios more plausible. Other sources of geometries with nontrivial topology are brane worlds. In this context, the wormhole is supported by the influence of a bulk in the brane which describes our Universe. It is in this framework that the present paper is inserted.

In this work we derive a family of asymptotically de Sitter wormhole solutions in a brane world context, more specifically in a Randall-Sundrum-type model [19]. We used the effective gravitational field equations derived by Shiromizu, Maeda, and Sasaki [20]. As there are few satisfactory bulk solutions for compact objects in Randall-Sundrum scenarios, one alternative is to build geometries in the brane and invoke Campbell-Magaard theorems [21], which guarantees their extensions through the bulk (locally at least). This approach has been used by several authors [13–16,22], and we will be following it in the present work. Moreover, global regularity of the brane is expected to facilitate the construction of a regular bulk solution [14]. This issue will be explored in the space-times constructed here.

Contrary to what has been suggested in the literature [15,23], we obtain de Sitter solutions which are regular everywhere. The class of geometries studied here complement the asymptotically flat space-times treated in [13–16,22]; and the asymptotically anti-de Sitter metrics in [23–25]. We should mention that solutions of the effective Einstein equations with positive cosmological constant in a brane setting were previously considered in [16]. While there is some overlap between the present work and [16], we have explored some global issues not considered in the mentioned paper, such as regularity and the existence of cosmological horizons. As will be discussed, these points are particularly important for de Sitter geometries.

If one considers the possibility of the existence of wormholes seriously, characteristics such as stability and response of wormholes to external perturbations should be investigated. Perturbative dynamics around wormholes [26] have not been as thoroughly explored as the black hole problem. We further advance the perturbative treatment of wormhole geometries in the present work. Matter and gravitational perturbations are considered in the background of the de Sitter wormhole geometries derived here.

The structure of this paper is presented in the following. In Sec. II we have derived a family of analytic asymptotically de Sitter solutions in a Randall-Sundrum-type brane. In Sec. III the maximal extensions of the solutions are considered and the wormhole geometries discussed. The near extreme limit of the wormhole solutions are considered in Sec. IV. Section V deals with the perturbative

*cmolina@usp.br
†juliano@fma.if.usp.br

analysis of the backgrounds derived. And finally, in Sec. VI some final remarks are made. In this work, we have used the metric signature diag$(-+++)$ and the geometric units $G_{4D} = c = 1$, where G_{4D} is the effective four-dimensional gravitational constant.

II. DE SITTER BRANE SOLUTIONS

The basic brane world set up is a four-dimensional brane, our Universe, immersed in a larger manifold, the bulk. It is generally postulated that the usual matter fields are confined in the brane [27]. Following the approach suggested by Shiromizu, Maeda, and Sasaki [20], the effective four-dimensional gravitational field equations in the vacuum Randall-Sundrum brane is

$$R_{\mu\nu} - \frac{1}{2} R g_{\mu\nu} = -\Lambda_{4D} g_{\mu\nu} - E_{\mu\nu}. \tag{1}$$

In this effective Einstein equation, Λ_{4D} is the four-dimensional brane cosmological constant and $E_{\mu\nu}$ is proportional to the (traceless) projection on the brane of the five-dimensional Weyl tensor. Eqs. (1) reduce to usual four-dimensional vacuum Einstein equations in the low-energy limit.

If we impose staticity and spherical symmetry in the brane, that is,

$$ds^2 = -A(r)dt^2 + \frac{dr^2}{B(r)} + r^2(d\theta^2 + \sin^2\theta d\phi^2), \tag{2}$$

the trace of Eq. (1) will be

$$R = 4\Lambda_{4D}, \tag{3}$$

where R denotes the four-dimensional Ricci scalar. The Eq. (3) may be written as a constraint between the functions A and B

$$2(1-B) - r^2 B\left\{\frac{A''}{A} - \frac{(A')^2}{2A^2} + \frac{A'B'}{2AB} + \frac{2}{r}\left[\frac{A'}{A} + \frac{B'}{B}\right]\right\} = 4\Lambda_{4D} r^2, \tag{4}$$

with prime ($'$) denoting differentiation with respect to r.

We propose to construct asymptotically de Sitter spacetimes, such that $\Lambda_{4D} > 0$. In addition, we assume that they are "close" to the usual spherically symmetric (electro) vacuum solution given by $A = A_0$ and $B = B_0$, with

$$A_0(r) = B_0(r) = 1 - \frac{2M}{r} + \frac{Q^2}{r^2} - \frac{\Lambda_{4D}}{3} r^2, \tag{5}$$

where M and Q^2 are positive constants. Denoting a particular solution by the pair (A, B) of functions which satisfy the constraint (4), we are searching for a family of solutions $\mathcal{S}$ such that:

(i) the vacuum solution (A_0, B_0) is an element of $\mathcal{S}$;

(ii) a generic solution $(A_{C_1}, B_{C_1}) \in \mathcal{S}$ is a continuous deformation of (A_0, B_0), that is, there is (at least) one set of solutions $\mathcal{D}_{C_1} = \{(A_C, B_C), 0 \le C \le C_1\}$, labeled by a real parameter C, such that $\mathcal{D}_{C_1} \subset \mathcal{S}$.

Since Eq. (4) is linear in terms of B, a linear combination of solutions with A fixed is still a solution. Moreover, since we are interested in deformations of the usual vacuum solutions, we assume the *Ansatz*

$$A(r) = A_0(r), \tag{6}$$

$$B(r) = B_0(r) - C B_{lin}(r), \tag{7}$$

with $\partial B_{lin}/\partial C = 0$. Using Eqs. (6) and (7), the constraint (4) can be rewritten as a linear first-order ordinary differential equation on the $B_{\rm lin}$

$$h(r)\frac{dB_{\rm lin}(r)}{dr} + f(r) B_{\rm lin}(r) = 0, \tag{8}$$

where the functions h and f are given by

$$h(r) = 4A_0 + rA_0', \tag{9}$$

$$f(r) = \frac{4A_0}{r} + 4A_0' + 2rA_0'' - \frac{r(A_0')^2}{A_0}. \tag{10}$$

The zero structure of h and A_0 will be of great importance. If $M > 0$, $Q \neq 0$ and $0 < \Lambda_{4D} < \Lambda_{\rm ext}$, where

$$\Lambda_{\rm ext} = \frac{3}{8Q^2} - \frac{1}{32}\left[\left(\frac{9M^2}{Q^3} - \frac{6}{Q}\right)^2 - 3M\left(\frac{9M^2}{Q^4} - \frac{8}{Q^2}\right)^{3/2}\right] \tag{11}$$

is the critical value of Λ_{4D}, the function A_0 has four real zeros r_c, r_+, r_- and r_n such that $r_n < 0 < r_- < r_+ < r_c$. Also in this region of the parameter space, the function h has four real zeros r_0, r_{0-}, r_{0--}, and r_{0n}, with $r_{0n} < 0 < r_{0--} < r_{0-} < r_0$. Explicit expressions for the several roots introduced are straightforward but cumbersome. Of fundamental importance in this work is the relation $r_+ < r_0 < r_c$, which is always satisfied for $0 < \Lambda_{4D} < \Lambda_{\rm ext}$.

The solution of (8) for the correction $B_{\rm lin}$, general up to a multiplicative integration constant, is given by

$$B_{\rm lin}(r) = A_0(r)\frac{(r - r_{0--})^{c_{0--}}}{(r - r_0)^{c_0}(r - r_{0-})^{c_{0-}}(r - r_{0n})^{c_{0n}}}, \tag{12}$$

where the positive constants c_0, c_{0-}, c_{0--} and c_{0n} are

$$c_0 = \frac{2}{\Lambda_{4D}}\frac{r_0(2\Lambda_{4D} r_0^2 - 1)}{(r_0 - r_{0-})(r_0 - r_{0--})(r_0 - r_{0n})}, \tag{13}$$

$$c_{0-} = -\frac{2}{\Lambda_{4D}}\frac{r_{0-}(2\Lambda_{4D} r_{0-}^2 - 1)}{(r_0 - r_{0-})(r_{0-} - r_{0--})(r_{0-} - r_{0n})}, \tag{14}$$

$$c_{0--} = -\frac{2}{\Lambda_{4D}}\frac{r_{0--}(2\Lambda_{4D} r_{0--}^2 - 1)}{(r_0 - r_{0--})(r_{0-} - r_{0--})(r_{0--} - r_{0n})}, \tag{15}$$

$$c_{0n} = -\frac{2}{\Lambda_{4D}}\frac{r_{0n}(2\Lambda_{4D} r_{0n}^2 - 1)}{(r_{0--} - r_{0n})(r_0 - r_{0n})(r_{0-} - r_{0n})}. \tag{16}$$

Therefore the complete solutions for A and B can be expressed as

$$A(r) = A_0(r) = \frac{\Lambda_{4D}}{3r^2}(r_c - r)(r - r_+)(r - r_-)(r - r_n), \quad (17)$$

$$B(r) = A_0(r)\left[1 - \frac{C}{(r - r_0)^{c_0}} \frac{(r - r_{0--})^{c_{0--}}}{(r - r_{0-})^{c_{0-}}(r - r_{0n})^{c_{0n}}}\right]. \quad (18)$$

It is apparent that the function B diverges in the limit $r \to r_0$. Since $r_+ < r < r_c$ is a natural candidate for the space-time static region and $r_+ < r_0 < r_c$, previous works in the literature [15,23] have suggested that regular de Sitter solutions of (3) might not exist. However, we will show that this is not so.

As will be discussed in the following sections, the main characteristics of this class of solutions are captured by the simpler case $M = Q = 0$. In this limit the coefficients r_c and r_0 can be easily expressed as

$$r_c = \sqrt{\frac{3}{\Lambda_{4D}}}, \qquad r_0 = \sqrt{\frac{2}{\Lambda_{4D}}}, \quad (19)$$

and $r_n = -r_0$, $r_{0n} = -r_0$, $c_0 = c_{0n} = 3/2$, $c_{0-} = 1$. The remaining constants r_-, r_{--}, r_{0-}, r_{0--} and c_{0--} are null. The metric functions are given by

$$A(r) = 1 - \frac{r^2}{r_c^2}, \quad (20)$$

$$B(r) = \left(1 - \frac{r^2}{r_c^2}\right)\left[1 - C\frac{1}{r(r^2 - r_0^2)^{3/2}}\right]. \quad (21)$$

The energy density, radial and tangential pressures associated with Eqs. (20) and (21) may be defined as

$$(-E^\nu_\mu) = 8\pi \begin{pmatrix} -\rho & & & \\ & p_r & & \\ & & p_t & \\ & & & p_t \end{pmatrix} \quad (22)$$

and are given by

$$8\pi\rho = \frac{C}{3r_0^2}\frac{2r^2 - 5r_0^2}{r(r^2 - r_0^2)^{5/2}}, \quad (23)$$

$$8\pi p_r = \frac{C}{r_0^2}\frac{2r^2 - r_0^2}{r^3(r^2 - r_0^2)^{3/2}}, \quad (24)$$

$$8\pi p_t = -\frac{C}{6r_0^2}\frac{4r^4 - 4r_0^2r^2 + 3r_0^4}{r^3(r^2 - r_0^2)^{5/2}}. \quad (25)$$

These energy density and pressures are not generally positive-definite, and the effective stress-energy tensor $(-E^\nu_\mu)$ do not satisfy usual energy conditions. Still, in the context of this work, they should be viewed as *effective quantities*, associated with a *vacuum* brane model.

III. WORMHOLES INSIDE COSMOLOGICAL HORIZONS

Strictly speaking, the metric described by the functions A and B in Eqs. (17) and (18), or in Eqs. (20) and (21), describes a space-time only for the values of the radial parameter r such that $A(r) > 0$ and $B(r) > 0$. The maximal extensions of these solutions will be presently treated. At this point, an important question to be treated is the range of the parameters for which the solution given by Eqs. (17) and (18) describes an acceptable geometry.

If $C < 0$, the functions A and B are positive for $r_+ < r < r_c$. But $r_+ < r_0 < r_c$, so B in Eq. (18) is divergent at r_0. The geometry is well-defined and static for $r > r_0$, but its curvature invariants are not bounded, as seen by the behavior of the Kretschmann scalar near r_0

$$\lim_{r \to r_0} |R_{\alpha\beta\gamma\delta}R^{\alpha\beta\gamma\delta}| \to \infty. \quad (26)$$

Therefore, for this case *a naked curvature singularity* is present at $r \to r_0$. This solution will not be further explored in the present work.

If $C = 0$, we recover the usual Reissner-Nordström-de Sitter vacuum solution, and the regular region is given by $r_+ < r < r_c$. As is well-known, in nonextremal regimes the surfaces $r = r_+$ and $r = r_c$ describe an event and a cosmological horizon in the maximal extension, respectively. One interpretation for this result is that, although the solutions with $C \neq 0$ and the Reissner-Nordström-de Sitter black holes have very different global characteristics, they nevertheless are locally arbitrarily close.

If $C > 0$, the function B is not positive-definite between r_+ and r_c. It has a third zero at $r = r_{\rm thr}$. The relevant point is

$$r_+ < r_0 < r_{\rm thr} < r_c, \quad (27)$$

with the functions A and B positive-definite and analytic for $r_{\rm thr} < r < r_c$. Therefore, the chart (t, r, θ, ϕ) is valid in the region $r_{\rm thr} < r < r_c$. The analytic extension beyond $r = r_{\rm thr}$ is suggested with the use of the proper length ℓ as radial function, where

$$\frac{d\ell(r)}{dr} = \frac{1}{\sqrt{B(r)}}. \quad (28)$$

Choosing an appropriate integration constant in Eq. (28), the region $r_{\rm thr} < r < r_c$ is mapped into $0 < \ell < \ell_{\rm max}$, with a finite $\ell_{\rm max}$. The extension is made analytic, continuing the metric with $-\ell_{\rm max} < \ell < \ell_{\rm max}$. The resulting geometry has a wormhole structure, with a throat at $r = r_{\rm thr}$.

The extension beyond $r = r_c$ can be made, for example, with the ingoing and outgoing Eddington charts (u, t, θ, ϕ) and (v, t, θ, ϕ), where u, v are the light-cone variables

$$u = t - r_\star \quad \text{and} \quad v = t + r_\star. \quad (29)$$

The radial variable $r_\star$ is the tortoise coordinate, defined as

$$\frac{dr_\star(r)}{dr} = \frac{1}{\sqrt{A(r)B(r)}}. \tag{30}$$

In the maximal extension, the surface $\ell = \ell_{\max}$ ($r = r_c$) is a Killing horizon, interpreted as a cosmological horizon. A more physical interpretation of the geometry is a spherically symmetric wormhole inside an exponentially expanding Universe.

Charts based on the tortoise coordinate $r_\star$ or the $u - v$ coordinates can be used to cover all the static region. In this case, $\{(t, \ell, \theta, \phi), \ell \in (-\ell_{\max}, +\ell_{\max})\}$ is mapped into $\{(t, r_\star, \theta, \phi), r_\star \in (-\infty, +\infty)\}$ or $\{(u, v, \theta, \phi), u \in (-\infty, +\infty), v \in (-\infty, +\infty)\}$. These coordinate systems will be used in the perturbative analysis of the wormhole.

Applying standard procedures (see, for example, [28]), the Penrose diagram of wormhole geometry can be obtained. This diagram is present in Fig. 1.

IV. THE NEAR EXTREME LIMIT

One limit where the geometry is simpler and its perturbative analysis is much easier (as we will see in the next section) is the near extreme regime. We will treat this limit in the present section.

In order that the background characterized by the metric functions (17) and (18) describes a wormhole, the real parameter C cannot be arbitrarily large. As C grows, $r_{\rm thr}$ approaches r_c. The extreme value for C ($C_{\rm ext}$), such that $\lim_{C\to C_{\rm ext}} r_{\rm thr} \to r_c$ with $0 < C < C_{\rm ext}$, is given by

$$C_{\rm ext} = \frac{(r_c - r_0)^{c_0}(r_c - r_{0-})^{c_{0-}}(r_c - r_{0n})^{c_{0n}}}{(r_c - r_{0--})^{c_{0--}}}. \tag{31}$$

We will consider in this section the *near extreme limit case*, where $C \lesssim C_{\rm ext}$, that is, C is very close (but still smaller) to the maximum value $C_{\rm ext}$. So, it is natural to define the dimensionless parameter

$$\delta = \frac{r_c - r_{\rm thr}}{r_c - r_0}. \tag{32}$$

With this definition, $0 < \delta < 1$, since $r_0 < r_{\rm thr} < r_c$. The near extreme regime can be characterized in terms of δ as the limit $0 < \delta \ll 1$. In fact, it can be shown that $C/C_{\rm ext} = 1 - \mathcal{O}(\delta)$.

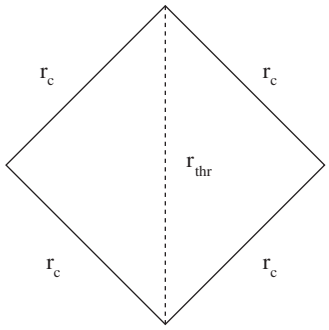

FIG. 1. Conformal diagram of wormhole the solution inside a cosmological horizon. Dashed line denotes the wormhole throat.

In the near extreme limit, the metric functions A and B can approximated by the linear and quadratic functions $A^{n-\rm ext}$ and $B^{n-\rm ext}$ respectively,

$$A(r) \approx A^{n\text{-ext}}(r) = A_0^{n\text{-ext}}(r_c - r), \tag{33}$$

$$B(r) \approx B^{n\text{-ext}}(r) = B_0^{n\text{-ext}}(r - r_{\rm thr})(r_c - r), \tag{34}$$

with the positive constants $A_0^{n-\rm ext}$ and $B_0^{n-\rm ext}$ given by

$$A_0^{n\text{-ext}} = \frac{\Lambda_{4D}}{3r_c^2}(r_c - r_+)(r_c - r_-)(r_c - r_n), \tag{35}$$

$$B_0^{n\text{-ext}} = A_0^{n\text{-ext}}\left(\frac{c_0}{r_c - r_0} + \frac{c_{0-}}{r_c - r_{0-}} - \frac{c_{0--}}{r_c - r_{0--}} + \frac{c_{0n}}{r_c - r_{0n}}\right). \tag{36}$$

It is important to stress that the causal structure of the space-time is not modified in the near extreme limit. The geometry still describes a wormhole inside cosmological horizons, with its Penrose diagram shown in Fig. 1. One important geometrical quantity is the surface gravity at the cosmological horizon. In the near extreme limit it can be explicitly calculated in terms of the roots of A and h

$$\kappa_c = \left|\frac{1}{2}\frac{d\sqrt{A(r)B(r)}}{dr}\right|_{r=r_c}\Bigg| = \frac{1}{2}\sqrt{A_0^{n\text{-ext}}B_0^{n\text{-ext}}(r_c - r_0)}\,\delta^{1/2}. \tag{37}$$

Although the cosmological horizons may be seen as close in the near extreme limit, this is not necessarily so. In fact, the proper radial distance between the horizons can be arbitrarily large even in the near extreme regime. Taking the case $M = Q = 0$ for simplicity, the maximum value for the radial proper distance ($\ell_{\max}$), half the proper distance between the two cosmological horizons, is $\ell_{\max} = 3\pi r_c/2$, which can be arbitrarily large as $r_c \to \infty$ ($\Lambda_{4D} \to 0$). The proper distance between horizons is then unbounded.

As discussed in previous and following sections, charts based on the tortoise coordinate introduced in Eq. (30) are very convenient for several applications. In the near extreme regime, the metric can be explicitly written in terms of $r_\star$

$$ds^2 = \delta A_0^{n\text{-ext}}(r_c - r_0)\,\mathrm{sech}^2(\kappa_c r_\star)(-dt^2 + dr_\star^2) + [r_c - \delta(r_c - r_0)\,\mathrm{sech}^2(\kappa_c r_\star)]^2 d\Omega_2^2. \tag{38}$$

V. PERTURBATIVE DYNAMICS AND STABILITY ANALYSIS

A. General considerations for the perturbative treatment

Once the background geometry is established, one next step is to determine its response under small perturbations. In the lowest order, background reaction can be ignored,

and the dynamics is restricted to the matter and gravitational perturbations in a fixed geometry. As a prototype of matter, we will consider massless and massive scalar fields, not necessarily minimally coupled to the background. The gravitational perturbation analysis will be limited here to the axial mode dynamics.

A massless scalar perturbation field Φ is characterized by the Klein-Gordon equation

$$\Box\Phi = 0. \tag{39}$$

Decomposing the scalar field Φ in terms of an expansion in spherical harmonic components

$$\Phi(t, r, \theta, \phi) = \sum_{l,m} \frac{\psi_l(t, r)}{r} Y_{lm}(\theta, \phi), \tag{40}$$

the Klein-Gordon equation give us a set of decoupled equations in the form

$$-\frac{\partial^2 \psi_l}{\partial t^2} + \frac{\partial^2 \psi_l}{\partial r_\star^2} = V_{\rm sc}(r(r_\star))\psi_l, \tag{41}$$

labeled by the multipole index l, with $l = 0, 1, 2, \ldots$. The tortoise coordinate $r_\star$ was introduced in Eq. (30), and Y_{lm} denotes the spherical harmonic functions. Using results in [29], the scalar effective potential is expressed in terms of r as

$$V_{\rm sc}(r) = \frac{l(l+1)}{r^2} A_0 + \frac{1}{r} A_0 A_0' - \frac{C}{2r}(A_0 B_{lin})'. \tag{42}$$

Typical profiles for the scalar effective potential are presented in Fig. 2.

We will consider gravitational perturbations in the brane geometry following the treatment in [29]. In general, the gravitational perturbations depend on the tidal perturbations, namely, first-order perturbations in $E_{\mu\nu}$ ($\delta E_{\mu\nu}$).

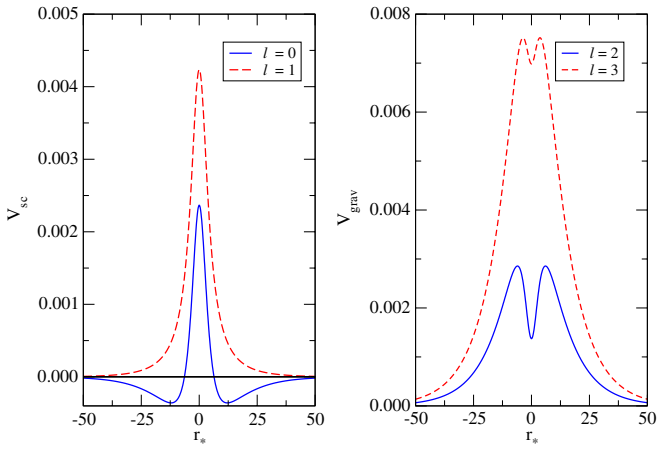

FIG. 2 (color online). Scalar and gravitational effective potentials (right and left panels, respectively) in terms of the tortoise coordinate $r_\star$. The wormhole parameters used in the plots were $\Lambda_{4D} = 0.01$, $M = 1.0$, $Q = 0.5$ and $\delta = 0.7$ ($r_{\rm thr} = 14.20$ and $r_c = 16.23$).

Since the complete bulk solution is not known, we shall use the simplifying assumption $\delta E_{\mu\nu} = 0$. This assumption can be justified at least in a regime where the energy carried in the perturbation processes does not exceed the threshold of the Kaluza-Klein massive modes [27]. Analysis of gravitational shortcuts [30,31] also supports this simplification, suggesting that gravitational fields do not travel deep into the bulk. Within these premises, the gravitational perturbation equation is

$$\delta R_{\mu\nu} = 0. \tag{43}$$

Following [29], the gravitational axial perturbations are given wave functions Z_l, satisfying a set of equations of motion with the form (45), labeled by a multipole index l ($l = 2, 3, \ldots$). The effective potential in this case is given by

$$V_{\rm grav}(r) = \frac{(l+2)(l-1)}{r^2} A_0 + \frac{2}{r^2} A_0^2 - \frac{1}{r} A_0 A_0' - C\left[\frac{2}{r^2} A_0 B_{\rm lin} - \frac{1}{2r}(A_0 B_{\rm lin})^2\right]. \tag{44}$$

Typical profiles are presented in Fig. 2.

Of particular interest in the perturbative dynamics are the so-called quasinormal mode spectra. Consider a wave function R, in the present case the scalar or gravitational perturbation (ψ_l or Z_l), subjected to an effective potential V ($V_{\rm sc}$ or $V_{\rm grav}$). The quasinormal modes are solutions of the "time-independent" version of Eq. (41),

$$\frac{\partial^2 \tilde{R}_\omega}{\partial r_\star^2} + (\omega^2 - V)\tilde{R}_\omega = 0, \tag{45}$$

satisfying both ingoing and outgoing boundary conditions asymptotically

$$\lim_{r_\star \to \mp\infty} \tilde{R}_\omega e^{\pm i\omega r_\star} = 1. \tag{46}$$

The "frequency domain" wave function $\tilde{R}_\omega$ associated with a given quasinormal mode ω is given by the Laplace transform [32] of the function R as

$$\tilde{R}_\omega(r_\star) = \int_0^\infty R(t, r_\star) e^{i\omega t} dt. \tag{47}$$

with ω extended to the complex plane.

The relevance of the quasinormal mode calculation is twofold. They determine the dynamical evolution of the wave function when the wave equation is subjected to bounded initial conditions. Moreover, $\mathrm{Im}(\omega) < 0$ is a necessary condition for the stability of the perturbation. The determination of quasinormal mode spectra for the wormhole geometry will be made with analytical and numerical techniques in the next subsections.

As will be discussed in the following, the dynamics of the perturbations considered can be analytically treated in the near extreme limit introduced in Sec. IV. Beyond this regime, numerical tools are necessary. In order to analyze

quasinormal mode phase and late-time behavior of the perturbations, we apply a numerical characteristic integration scheme based in the light-cone variables u and v in Eq. (29), used, for example, in [33–36].

B. Spherically symmetric scalar mode ($l = 0$)

The scalar field perturbation has a spherically symmetric ($l = 0$) mode. This mode is distinct because its associated effective potential is not positive-definite, as illustrated in Fig. 2. This point raises the question of whether the time evolution of the scalar field is stable. One important result of this work is that, in our extensive numerical investigation, the perturbation is always bounded, that is, *no unstable modes were observed*.

The presence of relevant negative peaks in the scalar potential with $l = 0$ is a potential complication for the calculation of the quasinormal frequencies. Nevertheless, the direct integration scheme used in [33–36] can be successfully employed in the present case. We will discuss in the following some important points observed in the scalar field evolution in the wormhole background considered.

A nonusual feature observed in the scalar dynamics is that the field ψ, for a fixed value of $r_\star$, tends to a non-null constant $\psi_0^{(0)}$ for large t:

$$\lim_{t\to\infty} \psi_{l=0} \to \psi_0^{(0)}. \tag{48}$$

This point is illustrated in Fig. 3. A similar qualitative behavior was observed in other de Sitter geometries [35,36].

In the near extreme regime, the late-time field evolution can be better explored. The intermediate- and late-time field evolution has the form

$$\psi_{l=0} \simeq \psi_0^{(0)} + \psi_0^{(1)} e^{-\kappa_c t}, \tag{49}$$

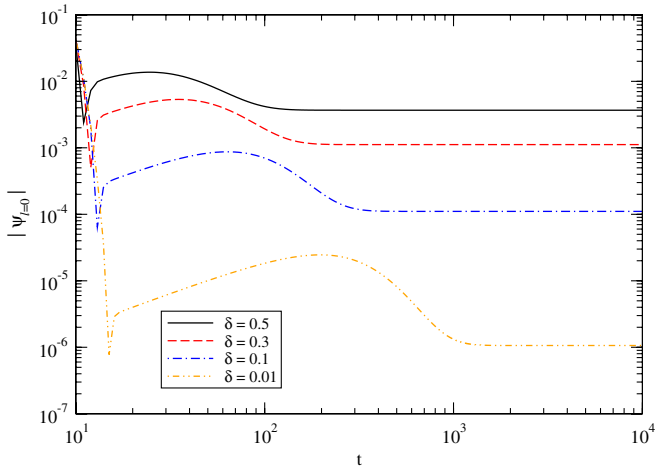

FIG. 3 (color online). Scalar field evolution with $l = 0$ and $r_\star = 0$, for several values of δ. For the wormhole geometries considered, the parameters $\Lambda_{4D} = 0.01$, $M = 1.0$ and $Q = 0.5$ ($r_c = 16.23$) were used.

with

$$\psi_0^{(0)} \propto \delta^2 \tag{50}$$

and κ_c denoting the surface gravity at the cosmological horizon, calculated at Eq. (37) in the near extreme limit. The dependence of $\psi_0^{(0)}$ with the parameter δ is illustrated in Fig. 4.

C. Higher multipole modes ($l > 0$)

A general feature of the effective potentials considered when $l > 0$ is that they are positive-definite. This point implies that *the dynamics is always stable for non-null l*. Other relevant characteristics of both potentials are the typically complicated profiles near $r_\star \approx 0$, as illustrated in Fig. 2. This latter point makes the WKB-based methods in [37–39] not effective in the present case, as explicitly checked by us. The direct integration schemes used in [33–36] can still be successfully employed. Analytic results will be available in the near extreme regime.

For the scalar perturbation with $l = 1$, the main qualitative characteristics of its perturbative dynamics are described as follows. If δ is close to 1 ($C/C_{\rm ext}$ small), the late-time decay is (nonoscillatory) exponential,

$$\psi_{l=1} \sim e^{kt}, \tag{51}$$

with $k < 0$. This result is consistent with the scalar dynamics around other asymptotically de Sitter geometries [34,35]. We illustrate this result in Fig. 5. For smaller values of δ (larger $C/C_{\rm ext}$), the decay is oscillatory, with an exponential envelope,

$$\psi_{l=1} \sim e^{{\rm Im}(\omega_0^{\rm sc})t} e^{-i\,{\rm Re}(\omega_0^{\rm sc})t}, \tag{52}$$

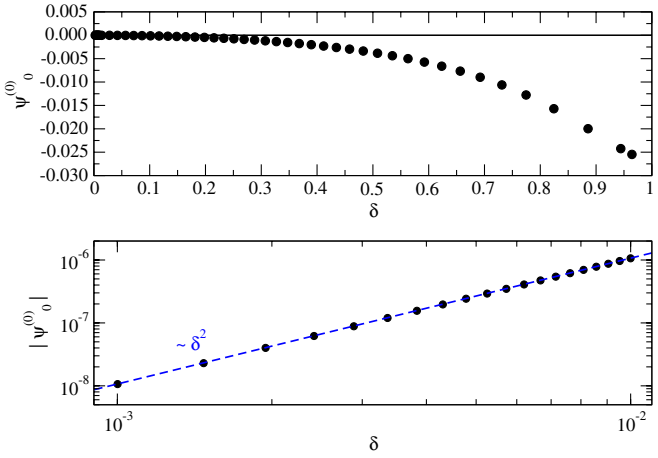

FIG. 4 (color online). Dependence of the asymptotic value for the $l = 0$ scalar mode ($\psi_0^{(0)}$) with the parameter δ. The bullets indicate numerical results, and the dashed line denotes a δ^2 power law. For the wormhole geometries considered, the parameters $\Lambda_{4D} = 0.01$, $M = 1.0$ and $Q = 0.5$ ($r_c = 16.23$) were used.

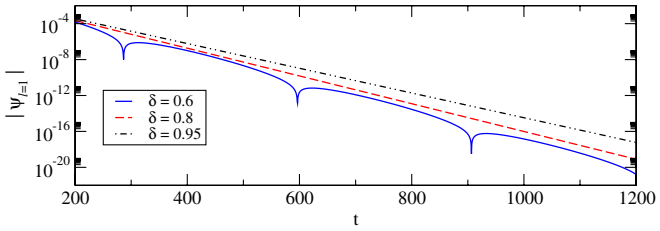

FIG. 5 (color online). Scalar field evolution with $l = 1$ and $r_\star = 0$, for several values of δ. For the wormhole geometries considered, the parameters $\Lambda_{4D} = 0.01$, $M = 0.1$ and $Q = 0.05$ ($r_c = 17.22$) were used.

where ω_0^{sc} is the fundamental (lowest absolute value of the imaginary part) quasinormal frequency associated with the $l = 1$ scalar mode and $\mathrm{Im}(\omega_0^{sc}) < 0$. We illustrate this result in Fig. 5.

Typical profiles for the dependence of the parameters k, $\mathrm{Im}(\omega_0^{sc})$ and $\mathrm{Re}(\omega_0^{sc})$ on δ are shown in Fig. 6. From these results, we see that the shift of oscillatory and nonoscillatory modes at $t \to \infty$ is determined by the relative magnitude of k and $\mathrm{Im}(\omega_0^{sc})$. If $|k| > |\mathrm{Im}(\omega_0^{sc})|$ (small δ), the nonoscillatory mode is suppressed for large t, and the oscillatory phase dominates. If $|\mathrm{Im}(\omega_0^{sc})| > |k|$ (large enough δ), the oscillatory mode is suppressed, and a late-time nonoscillatory decay is observed.

For scalar or gravitational perturbations with $l > 1$, the intermediate- and late-time dynamics is dominated by an oscillatory exponential decay. The scalar and gravitational perturbations can be well characterized by their fundamental quasinormal frequencies (ω_0^{sc} and ω_0^{grav}):

$$\psi_l \sim e^{-i\omega_0^{sc} t}, \tag{53}$$

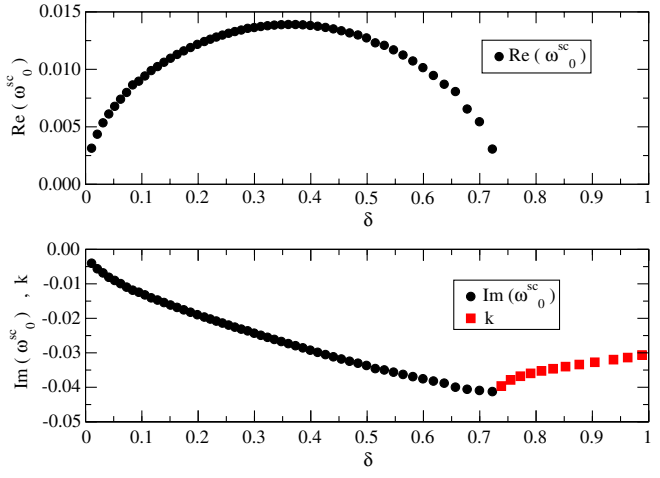

FIG. 6 (color online). Dependence of the exponential coefficient k and the scalar fundamental quasinormal frequency ω_0^{sc} on the parameter δ, for the $l = 1$ mode. For the wormhole geometries considered, the parameters $\Lambda_{4D} = 0.01$, $M = 0.1$ and $Q = 0.05$ ($r_c = 17.22$) were used.

$$Z_l \sim e^{-i\omega_0^{grav} t}. \tag{54}$$

These results are illustrated in Fig. 7. We have not observed nonoscillatory exponential decays for the scalar or gravitational perturbations with $l > 1$, considering values of C/C_{ext} as low as 10^{-4} ($\delta \approx 0.999$).

In the near extreme regime ($0 < \delta \ll 1$ or $C/C_{ext} \lesssim 1$), considered in Sec. IV, the scalar and gravitational quasinormal mode spectra can analytically determined. Explicit analytic expressions for the functions $V_{sc}(r(r_\star))$ and $V_{sc}(r(r_\star))$ are usually not available, except in particular, limits. One of these limits is the near extreme regime. Following an approach similar to the one used in [40,41], the result (38) allows both effective potentials to be written as

$$V(r(r_\star)) = \frac{V_{max}}{\cosh^2(\kappa_c r_\star)}, \tag{55}$$

with the surface gravity κ_c presented in Eq. (37). The constants V_{max}, for the scalar and gravitational perturbations (V_{max}^{sc} and V_{max}^{grav}, respectively) are

$$V_{max}^{sc} = \delta\Lambda_{4D} l(l+1) \times \frac{(r_c - r_0)(r_c - r_+)(r_c - r_-)(r_c - r_n)}{3r_c^4}, \tag{56}$$

with $l > 0$,

$$V_{max}^{grav} = \delta\Lambda_{4D}(l+2)(l-1) \times \frac{(r_c - r_0)(r_c - r_+)(r_c - r_-)(r_c - r_n)}{3r_c^4}, \tag{57}$$

with $l > 1$.

The potential in (55) is the so-called Pöschl-Teller potential [42]. It has been extensively studied, and, in

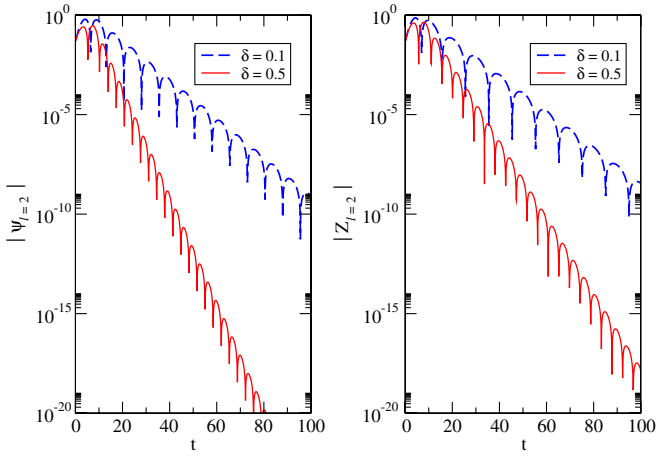

FIG. 7 (color online). Scalar and gravitational perturbations with $l = 2$ and $r_\star = 0$, for several values of δ. For the wormhole geometries considered, the parameters $\Lambda_{4D} = 3$ and $M = Q = 0$ ($r_c = 1$) were used.

particular, the quasinormal modes associated with it have been calculated [43,44]. Using the results in [43,44], we have for the scalar and gravitational quasinormal mode spectra, in the near extreme regime

$$\omega_n^{\mathrm{sc}} = \kappa_c \left[\sqrt{\frac{V_{\max}^{\mathrm{sc}}}{\kappa_c^2} - \frac{1}{4}} - \left(n + \frac{1}{2}\right) i \right], \tag{58}$$

$$\omega_n^{\mathrm{grav}} = \kappa_c \left[\sqrt{\frac{V_{\max}^{\mathrm{grav}}}{\kappa_c^2} - \frac{1}{4}} - \left(n + \frac{1}{2}\right) i \right]. \tag{59}$$

with κ_c, $V_{\max}^{\mathrm{sc}}$ and $V_{\max}^{\mathrm{grav}}$ given by expressions (37), (56), and (57) respectively.

The fundamental ($n = 0$) modes dominate the late-time decay. We stress the excellent concordance of the analytical expressions (58) and (59) with the numerical results in the near extreme regime. Moving away from the near extreme limit, we consider the quasinormal spectra for higher values of δ. A direct integration approach has been used. Quasinormal frequencies for the scalar and gravitational perturbations are presented in Tables I and II.

In all numerical calculations performed, the concordance between the numerical and near extreme approximation improves as δ is made smaller. This is a consistency check for the numerical results and an indication that the near extreme results are indeed adequate when the appropriate limit is taken. We illustrate this point in Tables I and II. Moreover, the analytical expression in Eq. (59) for the gravitational sector appears to work well even when the condition $\delta \ll 1$ is not strictly satisfied, as suggested by the data presented, for example, in Table II.

TABLE I. Fundamental quasinormal frequencies for the scalar perturbation for several values of δ and l. For the wormhole geometries considered, the parameters $\Lambda_{4D} = 3$ and $M = Q = 0$ ($r_c = 1$) were used. Relative errors ($\Delta\%$) for the near extreme results are indicated.

		Direct integration		Near extreme results	
l	δ	$\mathrm{Re}(\omega_0^{\mathrm{sc}})$	$\mathrm{Im}(\omega_0^{\mathrm{sc}})$	$\mathrm{Re}(\omega_0^{\mathrm{sc}})(\Delta\%)$	$\mathrm{Im}(\omega_0^{\mathrm{sc}})(\Delta\%)$
1	0.001	0.01660	−0.02143	0.01659(0.06%)	−0.02142(0.05%)
1	0.01	0.05224	−0.06806	0.05246 (0.42%)	−0.06773(0.49%)
1	0.1	0.1580	−0.2175	0.1659 (5.00%)	−0.2142(1.52%)
1	0.3	0.2318	−0.4130	0.2874 (24.0%)	−0.3710(10.2%)
1	0.5	0.2084	−0.5747	0.3710 (78.02%)	−0.4789(16.7%)
2	0.001	0.04177	−0.02143	0.04175 (0.05%)	−0.02142(0.05%)
2	0.01	0.1321	−0.06806	0.1320 (0.08%)	−0.06773(0.48%)
2	0.1	0.4192	−0.2248	0.4177 (0.36%)	−0.2143(4.67%)
2	0.3	0.7256	−0.4307	0.7232 (0.33%)	−0.3710(13.8%)
2	0.5	0.9157	−0.6025	0.9336 (1.95%)	−0.4789(20.5%)
2	0.7	1.017	−0.7086	1.105 (8.65%)	−0.5667(20.0%)
2	0.9	1.012	−0.9078	1.253 (23.8%)	−0.6426(29.2%)

TABLE II. Fundamental quasinormal frequencies for the gravitational perturbation for several values of δ and l. For the wormhole geometries considered, the parameters $\Lambda_{4D} = 3$ and $M = Q = 0$ ($r_c = 1$) were used. Relative errors ($\Delta\%$) for the near extreme results are indicated.

		Direct integration		Near extreme results	
l	δ	$\mathrm{Re}(\omega_0^{\mathrm{grav}})$	$\mathrm{Im}(\omega_0^{\mathrm{grav}})$	$\mathrm{Re}(\omega_0^{\mathrm{grav}})(\Delta\%)$	$\mathrm{Im}(\omega_0^{\mathrm{grav}})(\Delta\%)$
2	0.001	0.03178	−0.02141	0.03177 (0.03%)	−0.02142(0.05%)
2	0.01	0.1004	−0.06758	0.1005 (0.09%)	−0.06773(0.22%)
2	0.1	0.3167	−0.2095	0.3177 (0.32%)	−0.2142(2.24%)
2	0.3	0.5457	−0.3354	0.5503 (0.84%)	−0.3710(10.6%)
2	0.5	0.6962	−0.4383	0.7104 (2.04%)	−0.4789(9.26%)
2	0.7	0.8054	−0.5074	0.8405 (4.36%)	−0.5667(11.7%)
2	0.9	0.8647	−0.5622	0.9531 (10.2%)	−0.6426(14.7%)
3	0.001	0.05669	−0.02142	0.05668 (0.02%)	−0.02142(0.00%)
3	0.01	0.1792	−0.06778	0.1792 (0.0%)	−0.06773(0.07%)
3	0.1	0.5664	−0.2158	0.5667 (0.05%)	−0.2142(0.74%)
3	0.3	0.9785	−0.3803	0.9815 (0.31%)	−0.3710(2.24%)
3	0.5	1.254	−0.5012	1.267 (1.04%)	−0.4789(4.45%)
3	0.7	1.458	−0.6074	1.499 (2.81%)	−0.5667(6.70%)
3	0.9	1.577	−0.7013	1.700 (7.80%)	−0.6426(8.37%)

VI. FINAL REMARKS

We have obtained a family of exact solutions of the effective Einstein equations in an asymptotically de Sitter Randall-Sundrum brane. This family includes naked singularities, but also solutions which describe wormholes. Maximal extensions of the solutions were studied. We have shown that the extensions describe Lorentzian, traversable, wormhole space-times which connect regions bounded by cosmological horizons. It should be noted that, although the existence of a local, asymptotically de Sitter, solution for a metric in a Randall-Sumdrum scenario might be expected, it is not obvious that there would exist solutions regular everywhere. The explicit solutions constructed here have this characteristics.

One basic requirement, if the geometries obtained are to be considered as physically relevant, is the stability of the derived geometries under first-order perturbations. We have treated this question here considering scalar and axial gravitational perturbations. An important result in the perturbative analysis performed in this work is that *no unstable modes were found*.

Moreover, the detailed numerical and analytical treatment presented sketches a picture of the perturbative dynamics. Scalar spherically symmetric modes typically decay to a nonzero constant asymptotically. This is reminiscent of a feature already observed in considerations involving de Sitter black holes [34,35]. Although oscillatory and nonoscillatory decays bounded by exponential envelopes were observed, no power-law tails appeared, which also resembles the dynamics around asymptotically de Sitter black holes [34,35].

One interesting limit of the geometries derived in this work is their near extreme regime. This limit is interesting because the geometry becomes very simple, while still preserving the causal structure of the nonextreme case. In fact, in the near extreme regime the quasinormal spectra of the perturbations considered can be analytically determined, which is something not common in the literature. Moreover, the comparison between the full numerical results and the near extreme approximation shows good agreement for the fundamental overtone. We consider this result a strong argument for the validation of both approaches. Besides, the near extreme analytical results appear to describe reasonably well the gravitational quasinormal spectra even outside this limit.

ACKNOWLEDGMENTS

This work was partially supported by Conselho Nacional de Desenvolvimento Científico e Tecnológico (CNPq) and Coordenação de Aperfeiçoamento de Pessoal de Nível Superior (CAPES), Brazil.

[1] Matt Visser, *Lorentzian wormholes* (Springer-Verlag, New York, 1995).
[2] M. S. Morris and K. S. Thorne, Am. J. Phys. **56**, 395 (1988).
[3] Michael S. Morris, Kip S. Thorne, and Ulvi Yurtsever, Phys. Rev. Lett. **61**, 1446 (1988).
[4] José P. S. Lemos, Francisco S. N. Lobo, and Sérgio Quinet de Oliveira, Phys. Rev. D **68**, 064004 (2003).
[5] C. Molina, Prado Martin-Moruno, and Pedro F. Gonzalez-Diaz, Phys. Rev. D **84**, 104013 (2011).
[6] B. Bhawal and S. Kar, Phys. Rev. D **46**, 2464 (1992).
[7] G. Dotti, J. Oliva, and R. Troncoso, Phys. Rev. D **75**, 024002 (2007).
[8] A. G. Agnese and M. La Camera, Phys. Rev. D **51**, 2011 (1995).
[9] L. A. Anchordoqui, S. E. Perez Bergliaffa, and D. F. Torres, Phys. Rev. D **55**, 5226 (1997).
[10] K. K. Nandi, B. Bhattacharjee, S. M. K. Alam, and J. Evans, Phys. Rev. D **57**, 823 (1998).
[11] K. K. Nandi, A. Islam, and J. Evans, Phys. Rev. D **55**, 2497 (1997).
[12] Francisco S. N. Lobo and Miguel A. Oliveira, Phys. Rev. D **81**, 067501 (2010).
[13] R. Casadio, A. Fabbri, and L. Mazzacurati, Phys. Rev. D **65**, 084040 (2002).
[14] K. A. Bronnikov and Sung-Won Kim, Phys. Rev. D **67**, 064027 (2003).
[15] K. A. Bronnikov, V. N. Melnikov, and H. Dehnen, Phys. Rev. D **68**, 024025 (2003).
[16] Francisco S. N. Lobo, Phys. Rev. D **75**, 064027 (2007).
[17] A. G. Riess *et al.* (Supernova Search Team Collaboration), Astron. J. **116**, 1009 (1998); S. Perlmutter *et al.* (Supernova Cosmology Project Collaboration), Astrophys. J. **517**, 565 (1999).
[18] Robert R. Caldwell, Marc Kamionkowski, and Nevin N. Weinberg, Phys. Rev. Lett. **91**, 071301 (2003).
[19] L. Randall and R. Sundrum, Phys. Rev. Lett. **83**, 4690 (1999).
[20] T. Shiromizu, K. I. Maeda, and M. Sasaki, Phys. Rev. D **62**, 024012 (2000).
[21] Sanjeev S. Seahra and Paul S. Wesson, Classical Quantum Gravity **20**, 1321 (2003).
[22] N. Dadhich, R. Maartens, P. Papadopoulos, and V. Rezania, Phys. Lett. B **487**, 1 (2000).
[23] C. Molina and J. C. S. Neves, Phys. Rev. D **82**, 044029 (2010).
[24] José P. S. Lemos and Francisco S. N. Lobo, Phys. Rev. D **69**, 104007 (2004).
[25] Carlos Barceló, Luis J. Garay, Pedro F. González-Díaz, and Guillermo A. Mena Marugán, Phys. Rev. D **53**, 3162 (1996).
[26] R. A. Konoplya and C. Molina, Phys. Rev. D **71**, 124009 (2005); Necmi Bugdayci, Int. J. Mod. Phys. D **15**, 669 (2006); Vitor Cardoso, Paolo Pani, Mariano Cadoni, and Marco Cavaglià, Classical Quantum Gravity **25**, 195010 (2008); R. A. Konoplya and A. Zhidenko, Phys. Rev. D **81**, 124036 (2010); K. A. Bronnikov, J. C. Fabris, and A. Zhidenko, Eur. Phys. J. C **71**, 1791 (2011).
[27] Roy Maartens, Living Rev. Relativity **7**, 7 (2004), http://relativity.livingreviews.org/Articles/lrr-2004-7.
[28] M. Walker, J. Math. Phys. (N.Y.) **11**, 2280 (1970).
[29] E. Abdalla, B. Cuadros-Melgar, A. B. Pavan, and C. Molina, Nucl. Phys. **B752**, 40 (2006).
[30] E. Abdalla, B. Cuadros-Melgar, S.-S. Feng, and B. Wang, Phys. Rev. D **65**, 083512 (2002).
[31] E. Abdalla, A. G. Casali, and B. Cuadros-Melgar, Int. J. Theor. Phys. **43**, 801 (2004).
[32] H. P. Nollert and B. G. Schmidt, Phys. Rev. D **45**, 2617 (1992).
[33] C. Gundlach, R. H. Price, and J. Pullin, Phys. Rev. D **49**, 883 (1994).
[34] Patrick R. Brady, Chris M. Chambers, William Krivan, and Pablo Laguna, Phys. Rev. D **55**, 7538 (1997).
[35] C. Molina, D. Giugno, E. Abdalla, and A. Saa, Phys. Rev. D **69**, 104013 (2004).
[36] R. A. Konoplya, A. Zhidenko, and C. Molina, Phys. Rev. D **75**, 084004 (2007).
[37] B. F. Schutz and C. M. Will, Astrophys. J. **291**, L33 (1985).
[38] S. Iyer and C. M. Will, Phys. Rev. D **35**, 3621 (1987).
[39] R. A. Konoplya, Phys. Rev. D **68**, 024018 (2003).
[40] V. Cardoso and J. P. S. Lemos, Phys. Rev. D **67**, 084020 (2003).
[41] C. Molina, Phys. Rev. D **68**, 064007 (2003).
[42] G. Pöschl and E. Teller, Z. Phys. **83**, 143 (1933).
[43] V. Ferrari and B. Mashhoon, Phys. Rev. D **30**, 295 (1984).
[44] H. Beyer, Commun. Math. Phys. **204**, 397 (1999).